Structural insights into binding of STAC proteins to voltage-gated calcium channels

Siobhan M. Wong King Yuen[a,b], Marta Campiglio[c], Ching-Chieh Tung[a,b], Bernhard E. Flucher[c], and Filip Van Petegem[a,b,1]

[a]Department of Biochemistry and Molecular Biology, University of British Columbia, V6T 1Z3 Vancouver, BC, Canada; [b]The Life Sciences Centre, University of British Columbia, V6T 1Z3 Vancouver, BC, Canada; and [c]Department of Physiology and Medical Physics, Medical University of Innsbruck, 6020 Innsbruck, Austria

Edited by Kurt G. Beam, University of Colorado, Denver, Aurora, CO, and approved September 28, 2017 (received for review June 1, 2017)

Excitation–contraction (EC) coupling in skeletal muscle requires functional and mechanical coupling between L-type voltage-gated calcium channels ($Ca_V1.1$) and the ryanodine receptor (RyR1). Recently, STAC3 was identified as an essential protein for EC coupling and is part of a group of three proteins that can bind and modulate L-type voltage-gated calcium channels. Here, we report crystal structures of tandem-SH3 domains of different STAC isoforms up to 1.2-Å resolution. These form a rigid interaction through a conserved interdomain interface. We identify the linker connecting transmembrane repeats II and III in two different Ca_V isoforms as a binding site for the SH3 domains and report a crystal structure of the complex with the STAC2 isoform. The interaction site includes the location for a disease variant in STAC3 that has been linked to Native American myopathy (NAM). Introducing the mutation does not cause misfolding of the SH3 domains, but abolishes the interaction. Disruption of the interaction via mutations in the II–III loop perturbs skeletal muscle EC coupling, but preserves the ability of STAC3 to slow down inactivation of $Ca_V1.2$.

STAC adaptor proteins | voltage-gated calcium channel | muscle excitation–contraction coupling | disease mutation | X-ray crystallography

Muscle excitation–contraction (EC) coupling requires a functional interaction between an L-type voltage-gated calcium channel (1) (Ca_V), located in the plasma membrane, and the ryanodine receptor (RyR) (2), located in the sarcoplasmic reticulum (SR). Depolarization of the T-tubular membrane triggers release of Ca^{2+} from the SR, leading to muscle contraction.

For skeletal muscle, multiple studies have shown that RyR1 and $Ca_V1.1$ are coupled mechanically, with $Ca_V1.1$ serving as the voltage sensor for RyR1 (3–7). Conversely, changes in RyR1 can also affect the function of $Ca_V1.1$ (8, 9). Freeze-fracture studies show particles, thought to correspond to $Ca_V1.1$ channels, grouped into tetrads, opposite foot structures corresponding to RyR1 (5, 10). However, whether $Ca_V1.1$ interacts with RyR1 directly, through auxiliary proteins, or a combination of both remains to be confirmed.

The protein STAC3 has been identified as a factor required for myogenic differentiation (11, 12). Recently, two groups independently identified STAC3 as a novel component essential for skeletal muscle EC coupling (13, 14). It belongs to a small family of three proteins in the SH3- and cysteine-rich containing adaptor proteins (STAC1, STAC2, and STAC3). STAC3 is mostly expressed in skeletal muscle, whereas STAC1 and STAC2 are expressed in a variety of tissues, including the brain (13).

Multiple roles have been identified for the STAC proteins. STAC3 allows for expression of $Ca_V1.1$ in the plasma membrane of heterologous cells (15) and increases membrane expression in myotubes (16, 17). Although $Ca_V1.1$ can also be expressed at the plasma membrane of heterologous cells in the presence of the Ca_V-γ1 subunit, the addition of STAC3 results in much higher current amplitudes (16). Another role is in EC coupling, because myotubes from STAC3 knockout mice, which still have some degree of $Ca_V1.1$ expression, have a drastically reduced EC coupling. In addition, zebrafish embryos that are null for STAC3 still have normal levels of $Ca_V1.1$, but display a highly reduced EC coupling (14). Finally, STAC2 and STAC3 have been shown to slow down inactivation of $Ca_V1.2$ (15), an isoform expressed in both the heart and the brain. This suggests a possible role for STAC proteins in Ca_V regulation outside of skeletal muscle.

STAC3 is the target for a disease mutation (W284S) linked to Native American myopathy (NAM). The mutation results in a large reduction in EC coupling (16). It was also found to reduce the recruitment of STAC3 into the skeletal muscle $Ca_V1.1$ complex (18).

The STAC proteins contain three predicted structured domains, including a C1 domain near the N terminus, flanked by regions of predicted intrinsic disorder, and two SH3 domains in the C-terminal half (Fig. 1*A*). Here, we report crystal structures of individual and tandem SH3 domains of different STAC isoforms. We identify a binding site in the loop connecting repeats II and III of $Ca_V1.1$ and $Ca_V1.2$ and show the importance of this interaction for EC coupling.

Results

The Tandem SH3 Domains Form a Rigid Interaction. All three STAC isoforms have a predicted set of SH3 domains (SH3-1 and -2) in their C-terminal half. We set out to solve high-resolution structures of the tandem SH3 domains of both STAC1 and STAC2, with resolutions of 2.4 and 1.2 Å, respectively (Fig. 1*A*). Each

Significance

Skeletal muscle contraction is a tightly orchestrated event that starts with the depolarization of the T-tubular membrane. At the center is a functional and mechanical coupling between two membrane proteins: L-type voltage-gated calcium channels, located in the plasma membrane, and ryanodine receptors, located in the membrane of the sarcoplasmic reticulum. How exactly these proteins associate has remained a mystery, but recent reports have highlighted a key role for the STAC3 adaptor protein in this process. Here, we provide structural snapshots of the three STAC isoforms and identify a cytosolic loop of two Ca_V isoforms as a functional interaction site. A mutation linked to Native American myopathy is at the interface and abolishes the interaction.

Author contributions: M.C., B.E.F., and F.V.P. designed research; S.M.W.K.Y., M.C., C.-C.T., B.E.F., and F.V.P. performed research; S.M.W.K.Y., M.C., B.E.F., and F.V.P. analyzed data; and M.C., B.E.F., and F.V.P. wrote the paper.

The authors declare no conflict of interest.

This article is a PNAS Direct Submission.

Data deposition: The atomic coordinates and structure factors have been deposited in the Protein Data Bank, www.pdb.org (PDB ID codes 6B25–6B29).

[1]To whom correspondence should be addressed. Email: filip.vanpetegem@gmail.com.

This article contains supporting information online at www.pnas.org/lookup/suppl/doi:10.1073/pnas.1708852114/-/DCSupplemental.

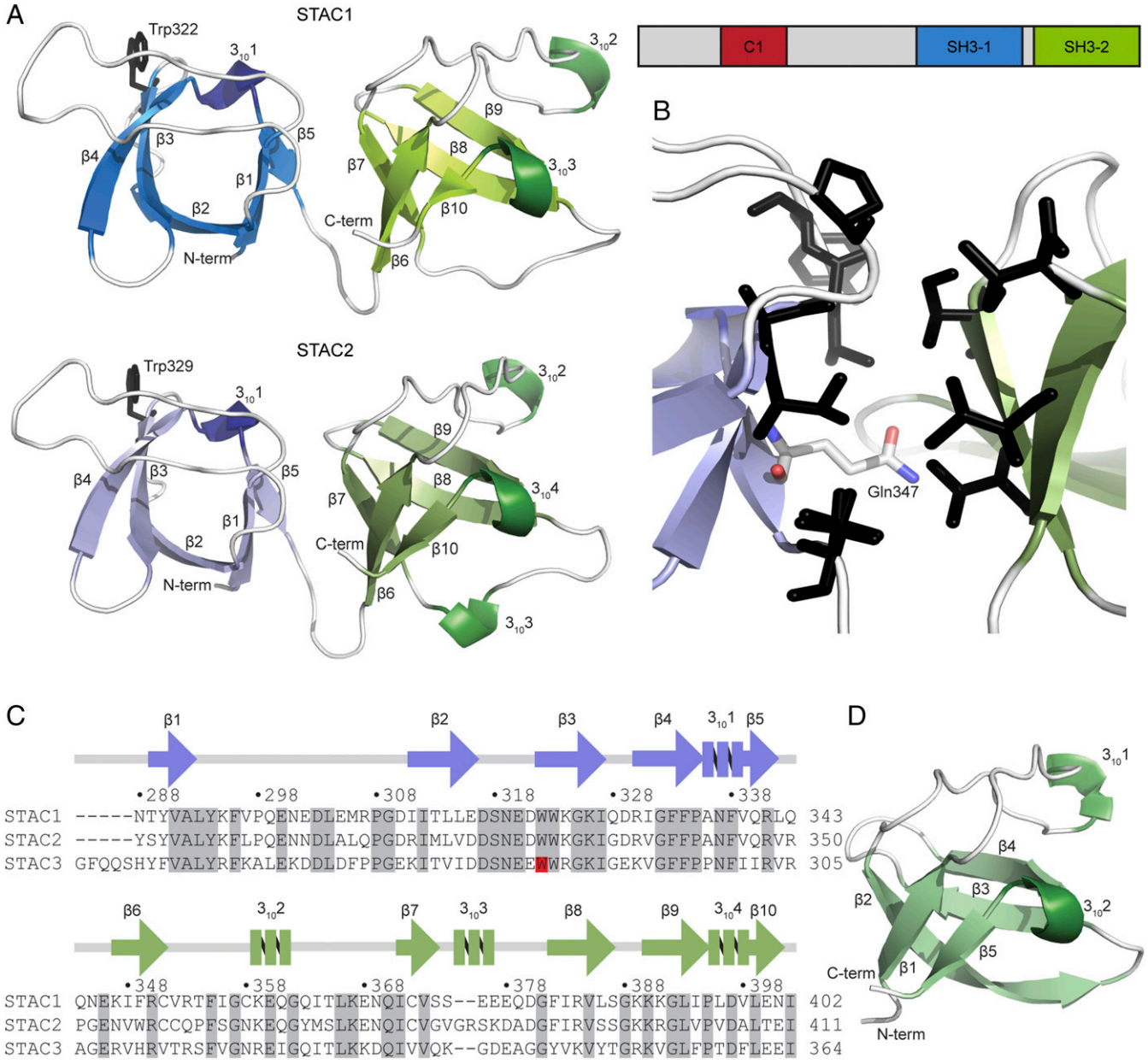

Fig. 1. Crystal structures of the STAC SH3 domains. (*A*) Schematic diagram of the domain arrangement within the STAC proteins (*Upper Right*). Crystal structures of the two tandem SH3 domains of STAC1 (*Upper Left*) and STAC2 (*Lower*) are shown. Beta-strands and 3_{10} helices are labeled. The conserved Trp residue implicated in NAM for STAC3 is shown in black sticks. (*B*) Close-up of the SH3 domain interface for STAC2, showing hydrophobic residues in black and Gln-347 in white sticks. (*C*) Sequence alignment of the SH3 domains of the three STAC isoforms with the secondary structure of STAC2 shown above. Trp-284 in STAC3 is highlighted in red. (*D*) Crystal structure of the second SH3 domain of STAC3.

domain consists of a five-stranded antiparallel β-sheet with additional short 3_{10} helices. SH3 domains are found in a plethora of proteins (19), but the STAC SH3 domains are unique because they are connected by a very short five-residue linker and form a rigid interaction through an extensive interdomain interface. In both isoforms, the relative domain orientation is very similar, shown by a superposition with a rmsd value of 1.28 Å for 104 Cα atoms (Fig. S1).

Fig. 1*B* shows the interdomain interface in STAC2. A big part of the interface is made up by hydrophobic residues, with the exception of Gln-347, located on the SH3-1 domain, which forms hydrogen bonds with main-chain atoms of the SH3-2 domain and water molecules. Gln-347 is conserved in human STAC1 and STAC2, but is replaced by an Ile in STAC3 (Fig. 1*C*). To verify its importance, we also solved a crystal structure of the Q347I mutant in STAC2. This structure superposes well with the wild-type STAC2, yielding an rmsd value of 0.62 Å for 80 superposed Cα atoms (Fig. S1), indicating that the Gln is not essential for maintaining the domain orientation. Since a similar interaction is seen in two different isoforms and for various molecules in the asymmetric unit, we conclude that this is a stable interface.

Although we have been unable to produce a structure of the STAC3 tandem SH3 domains, we did succeed in crystallizing its second SH3 domain (Fig. 1*D*). The resulting structure at 1.3 Å superposes very well with the SH3-2 domains of STAC1 and STAC2, with a rmsd value of 0.82 Å for 55 Cα atoms (based on

the superposition with STAC1). Previously, it had been suggested that STAC1 and STAC2 would lack a second SH3 domain (13, 18).

The Tandem SH3 Domains Interact with the II–III Linker of $Ca_V1.1$ and $Ca_V1.2$. In $Ca_V1.1$, the linker connecting transmembrane repeats II and III ("II–III loop") has been shown to be crucial for EC coupling (20–22). We therefore hypothesized that it may form a binding site for the STAC3 tandem SH3 domains. SH3 domains typically associate with proline-rich segments, and an interaction prediction server (23) suggested three putative sites within the loop, all contained within the fragment 728–775 (see Fig. 3*A*). Fig. 2*A* shows the results of isothermal titration calorimetry (ITC) experiments, where we titrated this fragment ("core II–III loop") into the STAC2 tandem SH3 domains. These show binding with a K_d of 1.85 μM. Both STAC1 and STAC3 also bind

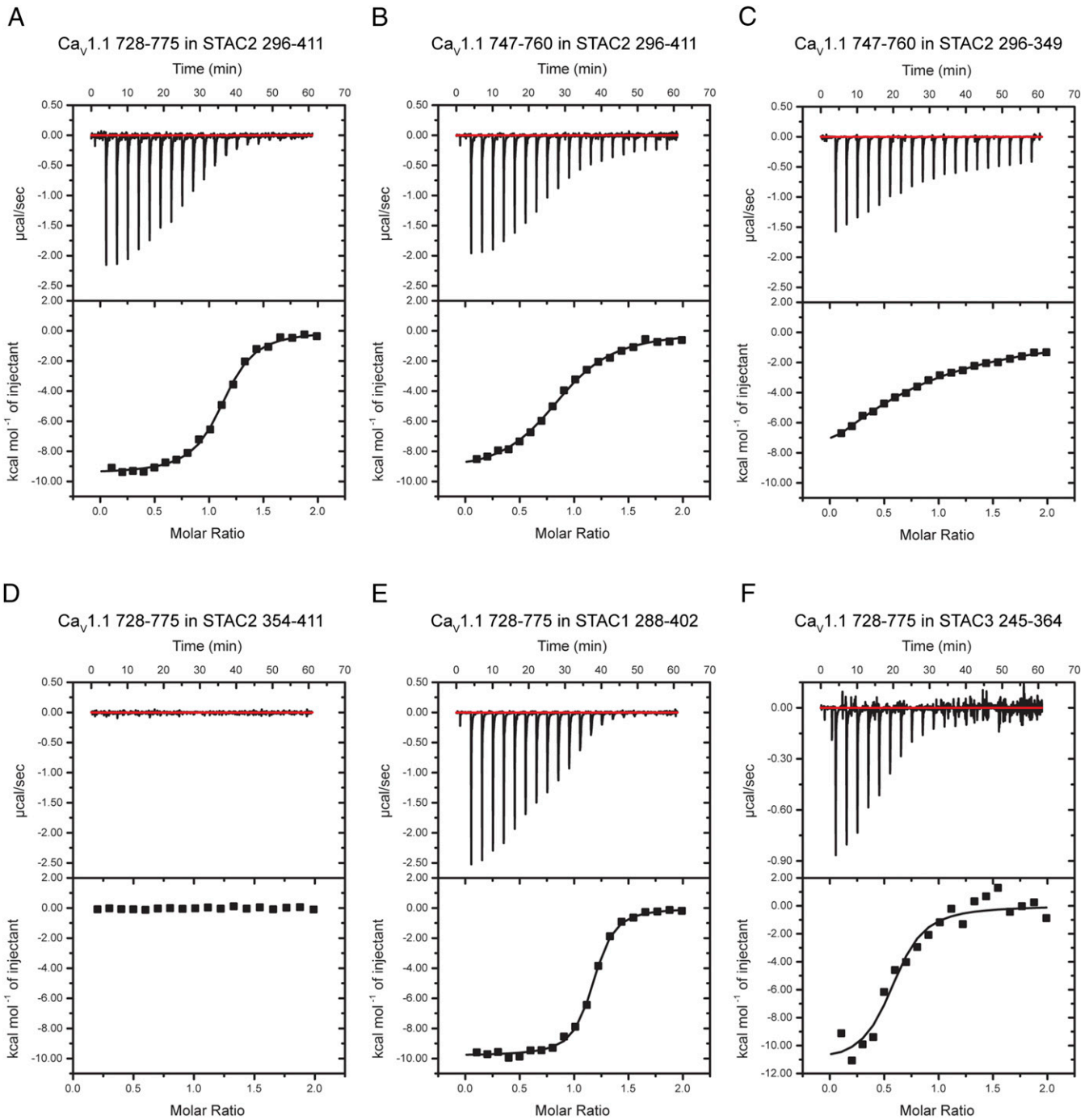

Fig. 2. ITC experiments reveal binding between peptides of the $Ca_V1.1$ II–III loop and the SH3 domains of the STAC proteins. (*A*) Shown is 1 mM $Ca_V1.1$ 728–775 (core II–III loop) titrated into 0.1 mM STAC2 tandem SH3 domains (residues 296–411). (*B*) Shown is 1 mM $Ca_V1.1$ 747–760 (minimal peptide) titrated into 0.1 mM STAC2 tandem SH3 domains. (*C*) Shown is 1 mM $Ca_V1.1$ 747–760 titrated into 0.1 mM STAC2 SH3-1 (residues 296–349). (*D*) Shown is 1 mM $Ca_V1.1$ 728–775 titrated into 0.1 mM STAC2 SH3-2 (residues 354–411). (*E*) Shown is 1 mM $Ca_V1.1$ 728–775 titrated into 0.1 mM STAC1 tandem SH3 domains (residues 288–402). (*F*) Shown is 390 μM $Ca_V1.1$ 728–775 titrated into 39 μM STAC3 tandem SH3 domains (residues 245–364).

to the same core II–III loop, with affinities ~2.4- and 2.2-fold higher than STAC2 (Fig. 2 *E* and *F* and Table S1).

We next tested binding of each predicted site individually to STAC3, but failed to detect any significant interaction with either peptide (Table S1). However, we noticed an additional set of proline residues next to the second predicted site and utilized a larger peptide, encoded by residues 747–760. This peptide showed binding to the tandem SH3 domains of STAC3 (K_d of 10.6 μM), as well as to STAC2 (9.3 μM) and STAC1 (3.9 μM) (Fig. 2 and Table S1). Since the peptide 747–760 is the shortest sequence for which we could detect reliable binding to STAC proteins, we call this the minimal peptide.

To determine whether the individual SH3 domains were required for binding, we utilized the individual domains of STAC2 for ITC experiments (Fig. 2 *C* and *D*). Only SH3-1 showed appreciable binding to the minimal peptide (K_d = 84 μM), but this affinity is lower compared with the construct containing both SH3 domains (K_d = 9.3 μM). The SH3-2 domain thus adds a small contribution, either by altering the conformation of the SH3-1 domain or by providing an additional interaction surface for the peptide.

To verify that the minimal peptide forms the main binding site within the core II–III loop, we generated a double mutant whereby Pro-756 and -758 were both mutated to alanine in the core II–III loop (residues 728–775). This mutant failed to show binding to STAC3, indicating that these prolines, contained within the minimal peptide, are a major binding determinant (Fig. S2*A*).

It was recently reported that STAC proteins can alter the function of $Ca_V1.2$ (15). We therefore tested whether the tandem SH3 domains could bind to a similar site in this channel isoform. Fig. S2*C* shows an ITC between the STAC2 tandem SH3 domains and the core II–III loop of $Ca_V1.2$ (equivalent to the core II–III loop of Ca_V 1.1). This interaction had a K_d of ~19 μM, representing a 10-fold weaker binding compared with $Ca_V1.1$. Fig. 3*A* shows a sequence alignment of the core II–III loop regions of all four Ca_V1 isoforms. Although we did not formally test binding to $Ca_V1.3$ and $Ca_V1.4$, based on sequence conservation, we predict that binding of the tandem SH3 domains may occur with the II–III loop of $Ca_V1.3$, but is unlikely to be significant for $Ca_V1.4$.

Many more proline-rich segments were present in the Ca_V sequences. We therefore also tested interactions between various cytosolic loops and termini of $Ca_V1.2$ with the STAC2 tandem SH3 domains. Together, the cytosolic segments tested cover all proline-rich regions predicted to bind SH3 domains (23), but no significant interactions could be detected outside of the II–III loop (Fig. S3). This suggests that the II–III loop is the primary binding site for the STAC SH3 domains.

Crystal Structure of STAC2 in Complex with a Peptide from the II–III Loop. We have solved a crystal structure of the STAC2 isoform in complex with the $Ca_V1.1$ minimal peptide (residues 747–760) at 1.73-Å resolution. The structure contains six complexes in the asymmetric unit, all with highly similar interfaces. Here, we describe the complex formed by STAC2 chain A, which showed the best density for the peptide. Although STAC2 is not coexpressed with $Ca_V1.1$ in skeletal muscle, the high conservation of the interface among STAC isoforms suggests a very similar interface for STAC3.

The interaction buries 547 $Å^2$ of surface area and mostly involves the SH3-1 domain (Fig. 3 *B* and *C* and Fig. S4*A*). Trp-329, conserved in all three STAC isoforms, is central in the interaction and is the target for a disease mutation linked to NAM in STAC3 (14). Its side-chain nitrogen forms a hydrogen bond with the main chain of the peptide.

On the $Ca_V1.1$ side, Arg-757 is involved in multiple interactions with SH3-1. It sits in a pocket lined by Trp-329 and is involved in an extensive hydrogen-bond network with Gln-306, Asp-310, and several additional water-mediated hydrogen bonds. It also forms an additional salt bridge with Glu-307 and a cation-pi interaction with Trp-329. Other interactions of interest are made by $Ca_V1.1$ residues Pro-753, which sits in another small pocket lined by Trp-329, and by Ile-752, which forms hydrophobic interactions. To show the importance of these residues, we mutated all three residues (Ile-752, Pro-753, and Arg-757) to alanines within the core II–III loop and were no longer able to detect an interaction with the STAC2 tandem SH3 domains (Fig. 3*D*).

Although we did not observe a direct interaction between the $Ca_V1.1$ peptide and the SH3-2 domain, the side chain of the $Ca_V1.1$ residue Glu-749 forms multiple water-mediated hydrogen bonds with STAC2, including Lys-374, located in the SH3-2 domain. This observation likely explains our observation that the tandem SH3 domains bind more strongly to this peptide than SH3-1 alone (Table S1). At the N terminus of the $Ca_V1.1$ peptide, two negatively charged residues display weak electron density that precluded building their structure. They would be pointing toward a highly positively charged region of the SH3-2 domain (Fig. 3*C*) and may thus also contribute to the affinity. We hypothesize that this additional interaction displays different conformational states, thus not providing clear electron density.

These interactions, described for STAC2, are most likely very similar for STAC1 and STAC3. First, all three isoforms were able to bind the same peptide (Fig. 2 and Table S1), and the surface residues of the binding region in STAC2 are highly conserved in STAC1 and STAC3 (Fig. 1*C*). The only exception is Gln-306, which is replaced by a Leu in STAC3. To test its importance in binding, we mutated Gln-306 to Leu in the STAC2 tandem SH3 domains and found the affinity for the minimal peptide to be approximately twofold lower than wild type (Table S1). So, although Gln-306 contributes to binding, it is not essential.

Because part of the SH3-2 surface seems to contribute to binding the II–III loop peptide, the question arises whether it may still bind a different peptide, residing either within or outside of $Ca_V1.1$. A closer inspection showed that the region of SH3-2 that interacts with the II–III loop peptide is not at the canonical binding surface for SH3 domains. Fig. S4*B* shows a superposition of the STAC2 SH3-2 domain with the structure of the SH3 domain of Abl, in complex with a target peptide [Protein Data Bank (PDB) ID code 3EG1]. This shows that the canonical contact interface resides distally away from the binding site for the short II–III loop peptide. Another peptide could thus bind to the canonical face of SH3-2, without clashing with the minimal II–III loop peptide, implying that the STAC tandem SH3 domains may bridge two discontinuous segments within $Ca_V1.1$, or possibly between $Ca_V1.1$ and another protein like RyR1. The tight association between the two SH3 domains would ensure a rigid link. However, the canonical Trp residue is replaced by a Phe in the SH3-2 domain (Phe-391 in STAC2; Fig. S4*B*). It thus remains to be determined whether the SH3-2 domain can form significant interactions on its own.

Effect of the NAM Mutation W284S. In STAC3, Trp-284 is the target for a disease mutation (W284S) linked to NAM (14). The equivalent residue in STAC2 is Trp-329, which forms the multiple interactions with the $Ca_V1.1$ peptide. We introduced the W284S mutation in STAC3, as well as the equivalent W329S mutation in STAC2. In both cases, we were still able to produce purified protein, indicating that the mutations did not cause complete misfolding of the domain. However, using ITC experiments, we were no longer able to detect an interaction with the II–III loop (Fig. 3*E*). One implication of this may be a loss of mechanical coupling to the skeletal muscle RyR1. This is in agreement with previous experiments showing that the W284S

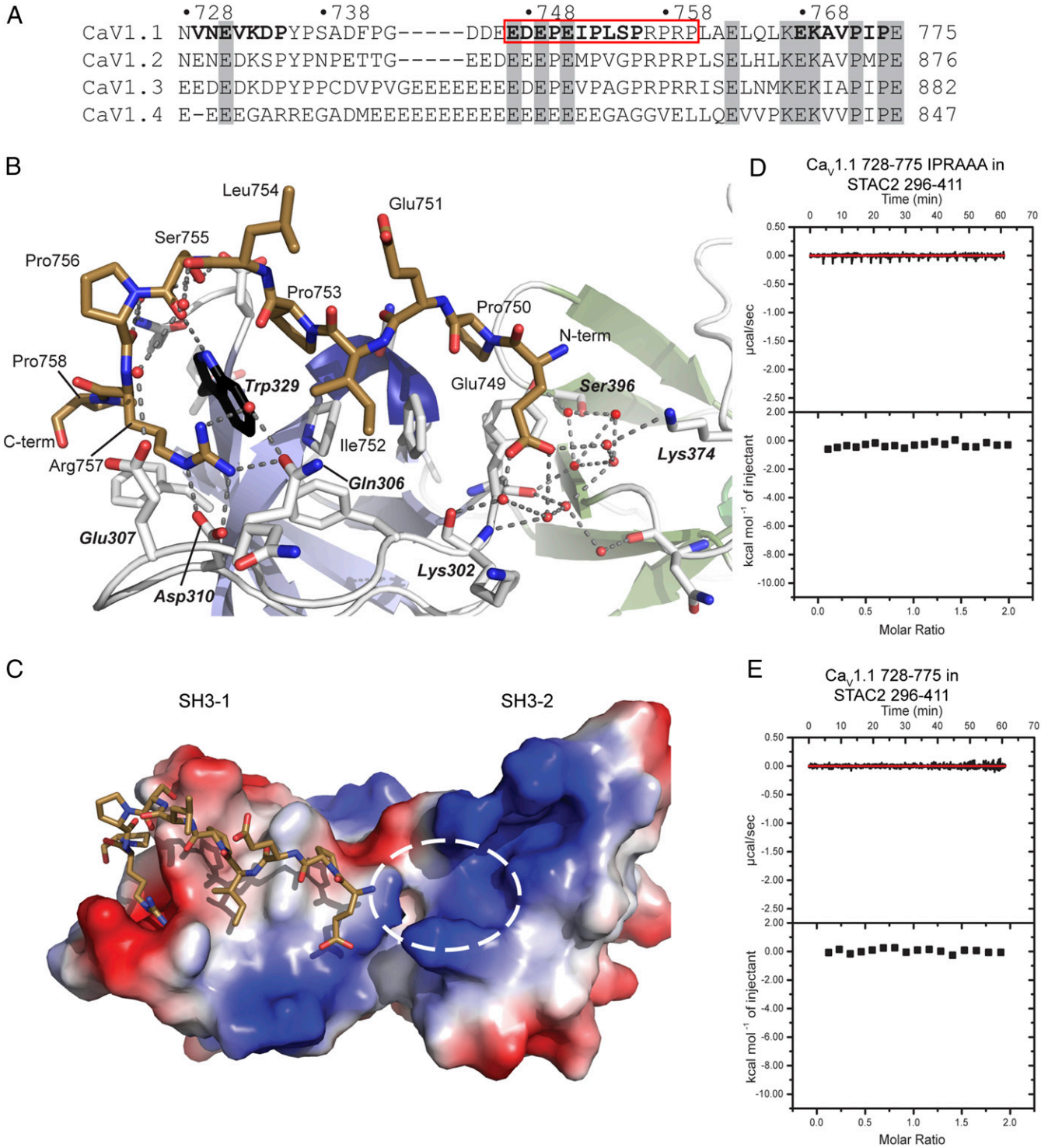

Fig. 3. Residues of the $Ca_V1.1$ core II–III loop have an extensive interaction network with the first SH3 domain of STAC2. (*A*) Sequence alignment of the cytosolic loop linking domains II and III in various Ca_V1 isoforms ($Ca_V1.1$–$Ca_V1.4$). Conserved residues are highlighted in gray. In bold are the three predicted SH3 binding sites. Outlined in the red box is the minimal peptide used in the complex of $Ca_V1.1$ and STAC2. (*B*) Crystal structure of the $Ca_V1.1$ 747–760 and STAC2 tandem SH3 domains complex. The $Ca_V1.1$ peptide is colored in gold with residue identities denoted in regular font. The key Trp329 STAC2 residue is colored in black. Critical STAC2 residues involved in the interaction with $Ca_V1.1$ are indicated in bold italic font. Ionic networks and water-mediated hydrogen-bond networks are indicated by dashed lines. (*C*) Electrostatic surface representation of the STAC2 tandem SH3 domains interacting with the $Ca_V1.1$ 747–760 peptide. The ellipse represents the region where we predict the N terminus of the $Ca_V1.1$ peptide, not visible in the crystal structure, would be located. (*D*) The core $Ca_V1.1$ II–III loop (residues 728–775, 1 mM) harboring the triple mutation, Ile-752A P753A R757A, dramatically diminished binding to the STAC2 tandem SH3 domains (residues 296–411, 0.1 mM). (*E*) ITC showing 1 mM $Ca_V1.1$ 728–775 (core II–III loop) titrated into 0.1 mM STAC2 tandem SH3 domains (residues 296–411) containing the W329S mutation (equivalent of the NAM mutation, W284S in STAC3). No significant binding was detected.

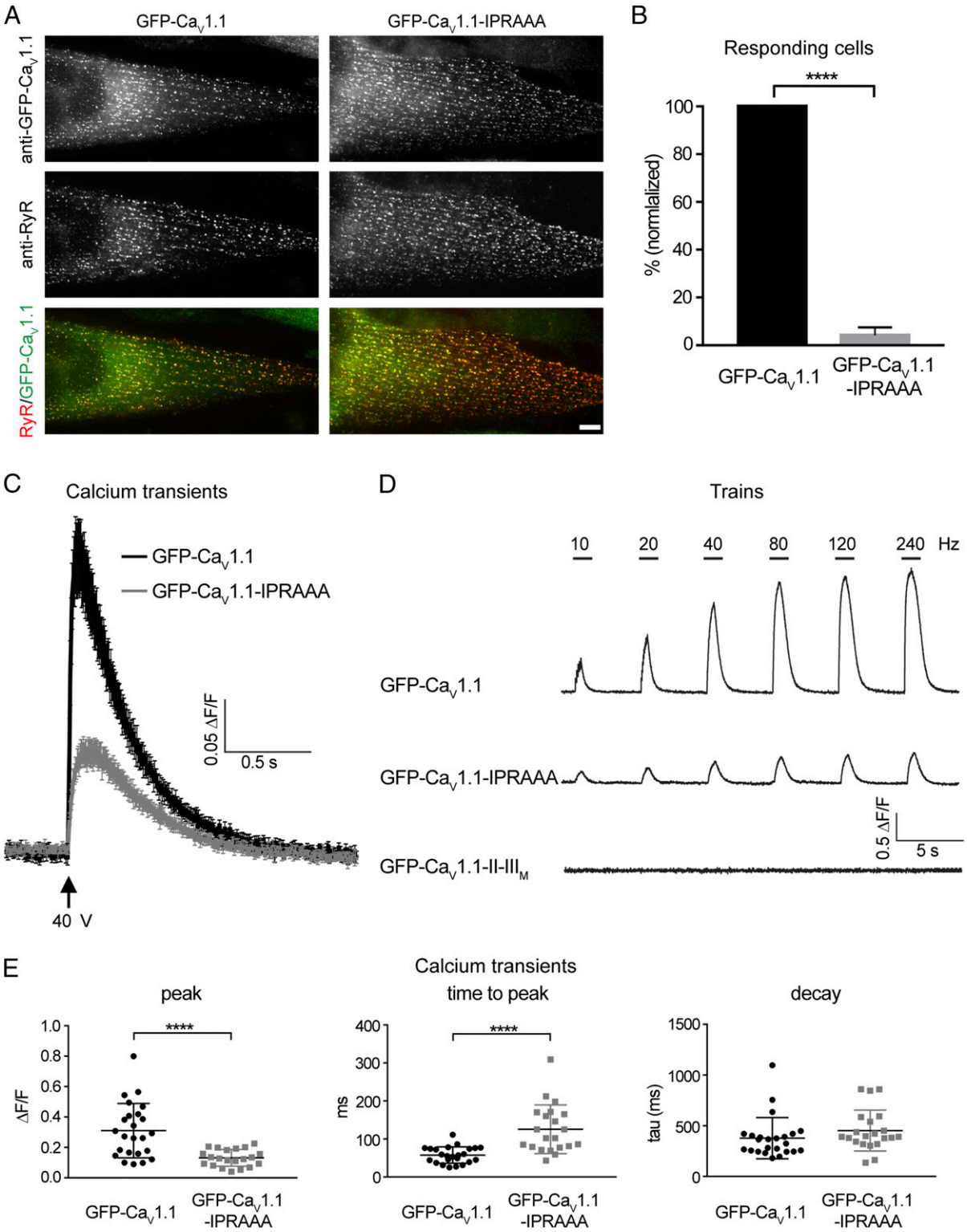

Fig. 4. Mutation of the IPR motif perturbs EC coupling in skeletal muscle myotubes. (*A*) Dysgenic ($Ca_V1.1^{-/-}$) myotubes reconstituted with GFP–$Ca_V1.1$ (*Left*) or the mutated GFP–$Ca_V1.1$–IPRAAA (*Right*) were double-immunolabeled with anti-GFP (*Top*) and anti-RyR (*Middle*). Clusters of GFP–$Ca_V1.1$ and GFP–$Ca_V1.1$–IPRAAA colocalized with the RyR1 (*Bottom,* yellow clusters in color overlay) indicate the correct targeting of both channel variants into t-tubule/SR or plasma membrane/SR junctions. (Scale bar, 10 μm.) (*B*) A severely reduced fraction of the cells transfected with GFP–$Ca_V1.1$–IPRAAA (4.1 ± 2.0%, *n*: three transfections, six dishes, $P < 0.0001$) responded with calcium transients to 2-ms pulses of 40 V, compared with cells transfected with GFP–$Ca_V1.1$. (*C*) Average calcium transients evoked by single 2-ms 40-V stimuli in myotubes expressing GFP–$Ca_V1.1$–IPRAAA (gray) or GFP–$Ca_V1.1$ (black). (*D*) GFP–$Ca_V1.1$–IPRAAA myotubes responded to tetanic stimulation up to 240 Hz, although with much reduced amplitudes, whereas myotubes reconstituted with the EC coupling-deficient mutant GFP–$Ca_V1.1$–II–III$_M$ showed no response at all. (*E*) Compared with GFP–$Ca_V1.1$, individual calcium transients in GFP–$Ca_V1.1$–IPRAAA expressing cells showed a significantly reduced peak amplitude ($P < 0.0001$; *Left*) and time to peak ($P < 0.0001$; *Center*), but comparable decay (*n*: four transfections, $n_{IPRAAA} = 21$, $n_{WT} = 24$; *Right*). Values are expressed as mean ± SEM. ****$P < 0.0001$ (unpaired *t* test).

mutation in STAC3 causes a drastic reduction in depolarization-induced calcium release in reconstituted *stac*$^{-/-}$ myotubes (16, 17).

Functional Role of the Interaction. If the SH3:II–III loop interaction is occurring in myocytes and of functional significance for EC coupling, then point mutations in the II–III loop that disrupt the interaction should have a functional effect similar to the NAM mutation. We therefore made use of the triple I752A/P753A/R757A mutation that knocks out binding to the tandem SH3 domains ($Ca_V1.1$–IPRAAA). We reconstituted dysgenic ($Ca_V1.1^{-/-}$) myotubes with wild-type and GFP–$Ca_V1.1$–IPRAAA and analyzed depolarization-induced calcium transients. Even though expression and triad targeting of the mutant construct was normal (Fig. 4*A*), the potency of GFP–$Ca_V1.1$–IPRAAA to reconstitute EC coupling was dramatically reduced compared with the wild-type control. The fraction of myotubes responding to electrical field stimulation with detectable calcium transients was only 4.1 ± 2.0% of cultures transfected with GFP–$Ca_V1.1$ (Fig. 4*B*). Moreover, in the few responding myotubes, calcium transients in response to single stimuli or to tetanic stimulation with increasing frequencies were significantly weaker with GFP–$Ca_V1.1$–IPRAAA than with GFP–$Ca_V1.1$ (Fig. 4 *C* and *D*). The peak amplitude of the transients was significantly reduced (0.13 ± 0.01 $\Delta F/F$) compared with control values (0.31 ± 0.04 $\Delta F/F$, $P < 0.0001$) and the time-to-peak was approximately doubled, from 57.6 ± 4.4 to 125.5 ± 14.0 ms ($P < 0.0001$) (Fig. 4*E*). In contrast, the decay of the calcium transient was not affected by the II–III loop mutations (377.5 ± 41.4 and 452.1 ± 44.1 ms, $P = 0.22$), indicating that overall calcium handling in the reconstituted myotubes was normal. In variance to the weak response of cultures reconstituted with GFP–$Ca_V1.1$–IPRAAA, transfection with GFP–$Ca_V1.1$–II–III_M, a II–III loop chimera known to lack skeletal muscle EC coupling (24), did not at all reconstitute depolarization-induced calcium transients in dysgenic myotubes (Fig. 4*D*). In summary, this analysis demonstrates that disruption of the interaction between the II–III loop of $Ca_V1.1$ and the tandem SH3 domains of STAC3 strongly perturbs skeletal muscle E-C coupling.

STAC3 has also been shown to affect inactivation of $Ca_V1.2$, causing a dramatic reduction in the speed of inactivation (15). However, neither mutations at the binding interface (W284S or IPRAAA) nor an outright deletion of both SH3 domains affected the slowing of inactivation induced by STAC3 (Fig. S5). We therefore conclude that the observed interaction between STAC proteins and the II–III loop is required for normal EC coupling (in the case of STAC3), but that slowing of inactivation is due to additional contact points beyond the tandem-SH3:II–III loop interaction, in agreement with a recent report highlighting the importance of the C1 domain (18).

Discussion

Skeletal muscle EC coupling relies on a mechanical link between the L-type calcium channel, $Ca_V1.1$, located in the plasma membrane, and RyR1, located in the SR membrane. Although several reports have suggested direct interactions between both proteins, an unambiguous interaction through a quantitative method or through structures of complexes have thus far been lacking (25). It is thus possible that the interaction is mediated, in full or in part, by auxiliary proteins. Recently, several reports have revealed a key function for the adaptor protein STAC3 (11–16, 18). A mutation in STAC3, W284S, is responsible for NAM, a rare disorder found in the Lumbee Native Americans (26). In addition to its role in EC coupling, STAC3 was also found to aid in expression of $Ca_V1.1$ at the plasma membrane of tsA201 cells (15) and to slow down inactivation of $Ca_V1.2$, an isoform found both in the heart and within neurons.

Here, we provide structural insights into the STAC proteins, by solving high-resolution crystal structures of the tandem SH3 domains of STAC1 and STAC2 and the second SH3 domain of STAC3. These domains form a compact arrangement by virtue of a short linker and form a micromolar affinity binding site for the II–III loops of $Ca_V1.1$ and $Ca_V1.2$. The binding site is located within a short proline-rich peptide encoded by residues 747–760 in human $Ca_V1.1$. The corresponding region also forms a binding site in $Ca_V1.2$.

We postulate that the interaction of the $Ca_V1.1$ II–III loop with the STAC3 tandem SH3 domains is required for EC coupling. Indeed, using field stimulation experiments in dysgenic myotubes, we show that a mutant $Ca_V1.1$, unable to bind the tandem SH3 domains via its II–III loop, severely perturbs skeletal muscle EC coupling (Fig. 4). This is also in agreement with reports that have shown the importance of the II–III loop in bidirectional coupling with RyR1 (20, 27, 28). The region 720–765, which encompasses the described binding site, was shown to be essential for normal EC coupling (24), and insertion of YFP immediately adjacent to the site, between residues 760 and 761, completely knocked out bidirectional coupling (29).

The structure also directly explains the effect of the W284S mutation in STAC3, responsible for NAM. The equivalent residue in STAC2, W329, forms key interactions with the II–III loop peptide, and either the W329S mutation in STAC2 or the W284S mutation in STAC3 decreases the affinity to levels below detection. Previous functional experiments have shown that the W284S mutation results in diminished EC coupling (16) and in reduced recruitment of STAC3 into the skeletal muscle $Ca_V1.1$ complex (18).

STAC2 and STAC3 have been shown to decrease the speed of inactivation of $Ca_V1.2$ (15), but the observed interaction does not appear necessary for this process. Even an outright deletion of both SH3 domains still resulted in slower inactivation, suggesting that slowing of inactivation is mediated either by the C1 domain or the intrinsically disordered regions flanking this domain. These results imply that one or more additional binding interfaces exist between STAC proteins and $Ca_V1.1$ or $Ca_V1.2$. Indeed, a recent report has shown that the C1 domain of STAC3 is crucial for the stability of the complex between STAC3 and L-type calcium channels (18). Whereas the NAM mutation did not appear to abolish the interaction between $Ca_V1.1$ and STAC3, mutation of only two residues in the C1 domain increased the turnover of STAC3 in skeletal muscle triads. The identity of the $Ca_V1.1$ and $Ca_V1.2$ segments interacting with the C1 domain remains to be described.

Could STAC3 be a protein that links both $Ca_V1.1$ and RyR1? Previous experiments have shown coimmunoprecipitation of STAC3 with RyR1 (14) in muscle tissue. However, recombinant STAC proteins expressed in dysgenic myotubes, which contain RyR1 but not $Ca_V1.1$, were not targeted into triad junctions (15, 18), and also photobleaching experiments in tsA201 cells could not confirm this interaction (15). It is still possible that there is a weak interaction between STAC3 and RyR1 in native cells, only occurring by virtue of a high local concentration. In our structure of the STAC2:$Ca_V1.1$ II–III loop peptide complex, the canonical binding surface of the SH3-2 domain is still available for binding another peptide (Fig. S4*B*). However, whether RyR1 and STAC3 interact remains to be determined.

In conclusion, STAC3 has emerged as a novel player in EC coupling, and our results provide insights into the specific interactions with $Ca_V1.1$. Further experiments will be required to identify additional binding sites within both $Ca_V1.1$ and other EC-coupling proteins.

Materials and Methods

Expression Constructs. All constructs for ITC and X-ray crystallography (Table S1) were cloned into a modified pET28 vector (Novagen), containing a His_6-tag, maltose-binding protein, and a cleavage site for the tobacco etch virus (TEV) protease (30). Table S2 outlines the exact constructs used. Cloning

procedures for GFP–$Ca_V1.1$ (NM_001101720) and GFP–$Ca_V1.1$–II–III_M were described (24, 31). Mutations of I752, P753, and R757 to alanines were introduced by splicing by overlap extension PCR. Briefly, the II–III loop cDNA sequence of $Ca_V1.1$ was amplified by PCR with overlapping mutagenesis primers in separate PCR reactions by using GFP–$Ca_V1.1$ as template. The two separate PCR products were then used as templates for a final PCR with flanking primers to connect the nucleotide sequences. This fragment was digested with SmaI/XhoI and cloned in the respective sites of GFP–$Ca_V1.1$, yielding GFP–$Ca_V1.1$–IPRAAA. Sequence integrity was confirmed by sequencing (MWG Biotech).

Protein Expression and Purification. Proteins were expressed for 20–24 h in *Escherichia coli* Rosetta (DE3) pLacI (Novagen) grown in 2× YT medium at 18 °C. Cells were lysed via sonication in 250 mM KCl and 10 mM Hepes (pH 7.4) (buffer A) supplemented with 1 mM PMSF, 25 μg/mL DNaseI, 25 μg/mL lysozyme, 10% glycerol, 6.2 mM β-mercapotoethanol (β-me), and 20 mM imidazole. Lysates were applied to HisTrap FF Crude columns (GE Healthcare), washed with 10 column volumes (CVs) of buffer A plus 20 mM imidazole, and eluted with buffer B (containing 250 mM KCl and 500 mM imidazole, pH 7.4). All $Ca_V1.1$ and Ca_V 1.2 constructs were further purified by an Amylose column (New England Biolabs), washed with 2 CVs of buffer A supplemented with 50 mM $CaCl_2$, and eluted with buffer A plus 10 mM maltose. Following cleavage of both the STAC and Ca_V proteins with His-tagged TEV protease for 12–14 h at 4 °C, dialyzing against buffer A supplemented with 3 mM β-me, the proteins were applied to a Talon column (Clontech) in buffer A and eluted with buffer B. The collected flow-through fractions were concentrated by using 3-kDa MWCO Amicon concentrators before loading onto a Superdex75 16/600 column (GE Healthcare) in buffer A supplemented with 2 mM Tris(2-carboxyethyl)phosphine (TCEP).

Crystallization and Structure Determination. The STAC3 SH3-2 domain was crystallized by using sitting-drop or hanging-drop vapor diffusion at room temperature by mixing equal volumes of protein (16 mg/mL) and well solution, containing 0.1 M Bis·Tris (pH 6.5), 22.5% (wt/vol) PEG 3350, and 0.2 M ammonium acetate. Crystals were soaked in a mixture of mother liquor and 30% ethylene glycol and flash-frozen. The tandem SH3 domain construct of STAC1 was crystallized by sitting-drop vapor diffusion at room temperature and by mixing equal volumes of protein (10 mg/mL) and well solution, which contained 0.1 M Na–Hepes (pH 7.5) and 25% (wt/vol) PEG 1000. Crystals were transferred to a cryosolution containing the mother liquor and 35% (vol/wt) glycerol and flash-frozen. The wild-type STAC2 tandem SH3 domain construct was crystallized in a 350-μL dialysis button against 150 mM KCl, 10 mM Hepes (pH 7.4), and 2 mM TCEP at 4 °C. Its complex with the synthetic minimal $Ca_V1.1$ peptide (obtained from LifeTein) was crystallized in a 1:2 ratio of STAC2:peptide by sitting-drop or hanging-drop vapor diffusion at 4 °C by mixing an equal amount of protein and well solution, which contained 2.24 M $(NH_4)_2SO_4$ and 0.1 M sodium acetate (pH 5.5). Before being flash-frozen in liquid nitrogen, the apo and complex STAC2 crystals were transferred to a drop containing mother liquor and 35 and 30% (vol/vol) glycerol, respectively. The STAC2 Q347I mutant was crystallized by hanging-drop vapor diffusion at 4 °C upon mixing equal volumes of protein (20 mg/mL) and well solution [0.1 M Bis·Tris, pH 6.4, 0.2 M lithium sulfate, and 35% (wt/vol) PEG 3350]. The Q347I mutant was cryoprotected with 25% PEG 200 and mother liquor. Diffraction data were collected at the Stanford Synchrotron Radiation Lightsource beamline BL9-2, the Advanced Photon Source beamline 23-ID-D, the Canadian Light Source beamline 08ID-1, and our homesource (Micromax 007 HF, Mar345 detector).

Data sets were processed by using XDS (32) and xia2. Initial phases were collected by iodide single-wavelength anomalous diffraction for the second SH3 domain of STAC3. Crystals of the second SH3 domain of STAC3 were soaked in 1 M NaI for 1–2 min before being frozen. Phases were determined via PHENIX (33); ARP/wARP was used to build an initial model of the structure of this individual domain; and the subsequent models were refined with PHENIX using high-resolution native datasets at 1.3 Å. The structure of apo-STAC2 (tandem SH3 domains) was solved by molecular replacement via Phaser (34), using the SH3-2 domain of STAC3 and an SH3 NMR structure (PDB ID code 2DL4) as search models. Structures of STAC2 Q347I, apo-STAC1, and the complexed STAC2 tandem SH3 domains were solved by molecular replacement using the structure of apo-STAC2 as a search model. All models were completed with iterative cycles of manual model building in Coot (35) and refinement with Refmac5 (36). All structure files are available in the PDB with accession codes 6B25, 6B26, 6B27, 6B28, and 6B29.

ITC. All proteins were concentrated and dialyzed against 150 mM KCl, 10 mM Hepes (pH 7.4), and 2 mM TCEP at 4 °C. The synthetic $Ca_V1.1$ peptide was dissolved in the dialysis buffer. Protein concentrations were determined by using a Nanodrop2000 spectrophotometer (Thermo Fisher). Titrations consisted of 20 injections of 2 μL with concentrations noted in the figure legends. Experiments were performed at 25 °C and using a stirring speed of 750 rpm on an ITC200 instrument (GE Healthcare). All data were processed by using Origin (Version 7.0), and isotherms were generated by following a point-by-point subtraction of a reference titration of ligand into buffer. STAC3 constructs were less stable compared with STAC2 and STAC1 and aggregated at higher concentration, thus reducing the effective concentration during ITC. The effective concentration of STAC3 for ITC with minimal peptide was therefore estimated by keeping the *N* value close to 1.

Immunolabeling. Myotubes of the homozygous dysgenic ($Ca_V1.1^{mdg/mdg}$) cell line GLT were cultured as described in Powell et al. (37). At the onset of myoblast fusion (2 d after addition of differentiation medium), GLT cultures were transfected by using *FuGene-HD* according to manufacturer's instructions (Promega). Cultures were fixed with paraformaldehyde 5 d after the transfection and double immunolabeled with rabbit anti-GFP (serum, 1:10,000; Molecular Probes) and mouse monoclonal anti-RyR (34-C; 1:1,000; Thermo Scientific) and fluorescently labeled with Alexa 488- and 594-conjugated secondary antibodies (Thermo Scientific), respectively. Samples were observed by using a 63×, 1.4-NA objective Axioimager microscope (Carl Zeiss Inc.), and 14-bit images were acquired with a cooled CCD camera (SPOT; Diagnostic Instruments) and Metaview image processing software. Images were arranged in Adobe Photoshop, and, where necessary, linear adjustments were performed to correct black level and contrast.

EC Coupling Analysis. Depolarization-induced calcium transients were recorded in 4- to 5-d posttransfection cultures loaded with 5 μM Fluo4-AM (Thermo Fisher) plus 0.1% Pluronic F-127 in Tyrode solution (130 mM NaCl, 2.5 mM KCl, 2 mM CaCl2, 2 mM MgCl2, 10 mM Hepes, and 30 mM glucose) for 40 min at room temperature. Calcium transients were elicited by passing 2-ms pulses of 40 V across the 19-mm incubation chamber, a condition approximately twofold above the stimulation threshold. In both conditions, myotubes showed a gradual response to increasing stimulation voltages (10–60 V), indicating that depolarization directly activated EC coupling without eliciting action potentials. Tetanic stimulation was performed with 500-ms trains of 2-ms 40-V stimuli at increasing frequencies between 10 and 240 Hz, in 4-s intervals. To analyze the efficacy of the $Ca_V1.1$ constructs to reconstitute EC coupling, the cover glasses were systematically scanned, and myotubes responding to continuous 0.5-Hz stimulation at 40 V were counted. Fluorescence signals from single myotubes were recorded with a PTI *RatioMaster* microphotometry system (Horiba Scientific). Traces were normalized by calculating the $\Delta F/F$ ratio in Microsoft Excel and analyzed with the Student *t* test in GraphPad. Results are expressed as mean ± SE, and graphs were assembled in GraphPad.

Electrophysiology. Constructs for electrophysiology consisted of human $Ca_V1.2$ (splice variant a1c77) in pcDNA3.1(+)/hygro (Invitrogen), rabbit Ca_V-β1 in pSP65, rabbit Ca_V-α2δ in pcDNA3 (Invitrogen), and human STAC3 isoform a (National Center for Biotechnology Information Reference Sequence NP_659501.1) in pcDNA3.1(–) (Invitrogen). STAC3 constructs encoded either the full-length transcript (1–364), a truncated STAC3 missing both SH3 domain (1–244), or a truncated STAC3 containing only the SH3 domains (residues 247–364). All RNA transcripts were prepared from cDNA by using a T7 mMessage mMachine kit except for Ca_V-β1, which was synthesized using a SP6 mMessage mMachine kit (Ambion). Collagenased *Xenopus leavis* stage V–VI oocytes were injected with 46.6 nL of a mixture containing 8.2–10.9 ng of $Ca_V1.2$ α1c and 11.7–15.5 ng of β1. Certain RNA mixtures, as described in the figure legends, were supplemented with 11.7 ng of Ca_V-α2δ and 9.8–13.0 ng of either of the STAC3 constructs described. Oocytes were kept at 18 °C in a modified Ringer's OR3 medium [50% (vol/vol) L-15 medium, 0.5% (vol/vol) L-glutamine, 0.5% (vol/vol) gentamycin, and 15 mM Hepes, adjusted to pH 7.6 using NaOH]. Recordings were performed 3–4 d following injection. Before recording, oocytes were injected with 50 nL of 500 mM of the tetrapotassium salt of 1,2-Bis(2-aminophenoxy)ethane-*N*,*N*,*N*′,*N*′-tetraacetic acid (ThermoFisher) to minimize contaminating Ca^{2+}-activated Cl^- current. Oocytes were then perfused by using a Ba^{2+}-containing solution [40 mM $Ba(OH)_2$, 50 mM NaOH, 1 mM KOH, and 10 mM Na–Hepes, adjusted to pH 7.4 using HNO_3] or a Ca^{2+}-containing solution [where the $Ba(OH)_2$ was replaced with $Ca(NO_3)_2$], as indicated in the figure legends. Two-electrode voltage-clamp experiments were performed by using an Axoclamp 900A amplifier (Molecular Devices) and digitized with a Digidata1440A digitizer (Molecular Devices). Electrodes were filled with 3 M KCl and had resistances of 0.1–1.2 MΩ. Ionic currents were collected and analyzed by using pClamp10; leak currents were subtracted using a P/4 protocol. Data were

normalized in Excel. Statistical significance was determined by using a two-tailed unpaired *t* test, with a confidence level of 95%. This analysis was performed and graphed by using GraphPad Prism 5.

All experimental procedures obtained approval of the University of British Columbia Biosafety Committee. No animals or human materials were used.

ACKNOWLEDGMENTS. We thank the support staff at the Advanced Photon Source (Chicago) GM/CA-CAT beamline 23-ID-D, the Stanford Synchrotron Radiation Lightsource (Menlo Park), and the Canadian Light Source (Saskatoon, SK, Canada), which is supported by the Natural Sciences and Engineering Research Council of Canada, the National Research Council Canada, the Canadian Institutes of Health Research (CIHR), the Province of Saskatchewan, Western Economic Diversification Canada, and the University of Saskatchewan. We also thank Liam Worrall for assistance with in-house data collection. This work was supported by CIHR Operating Grant MOP-119608 (to F.V.P.) and Austrian Science Fund (FWF) Grants T855 (to M.C.) and P27031 (to B.E.F.).

1. Zamponi GW, Striessnig J, Koschak A, Dolphin AC (2015) The physiology, pathology, and pharmacology of voltage-gated calcium channels and their future therapeutic potential. *Pharmacol Rev* 67:821–870.
2. Van Petegem F (2015) Ryanodine receptors: Allosteric ion channel giants. *J Mol Biol* 427:31–53.
3. Rios E, Brum G (1987) Involvement of dihydropyridine receptors in excitation-contraction coupling in skeletal muscle. *Nature* 325:717–720.
4. Tanabe T, Beam KG, Powell JA, Numa S (1988) Restoration of excitation-contraction coupling and slow calcium current in dysgenic muscle by dihydropyridine receptor complementary DNA. *Nature* 336:134–139.
5. Block BA, Imagawa T, Campbell KP, Franzini-Armstrong C (1988) Structural evidence for direct interaction between the molecular components of the transverse tubule/sarcoplasmic reticulum junction in skeletal muscle. *J Cell Biol* 107:2587–2600.
6. Adams BA, Tanabe T, Mikami A, Numa S, Beam KG (1990) Intramembrane charge movement restored in dysgenic skeletal muscle by injection of dihydropyridine receptor cDNAs. *Nature* 346:569–572.
7. Takekura H, Bennett L, Tanabe T, Beam KG, Franzini-Armstrong C (1994) Restoration of junctional tetrads in dysgenic myotubes by dihydropyridine receptor cDNA. *Biophys J* 67:793–803.
8. Nakai J, et al. (1996) Enhanced dihydropyridine receptor channel activity in the presence of ryanodine receptor. *Nature* 380:72–75.
9. Avila G, Dirksen RT (2000) Functional impact of the ryanodine receptor on the skeletal muscle L-type Ca(2+) channel. *J Gen Physiol* 115:467–480.
10. Franzini-Armstrong C, Protasi F, Ramesh V (1998) Comparative ultrastructure of Ca2+ release units in skeletal and cardiac muscle. *Ann N Y Acad Sci* 853:20–30.
11. Bower NI, et al. (2012) Stac3 is required for myotube formation and myogenic differentiation in vertebrate skeletal muscle. *J Biol Chem* 287:43936–43949.
12. Reinholt BM, Ge X, Cong X, Gerrard DE, Jiang H (2013) Stac3 is a novel regulator of skeletal muscle development in mice. *PLoS One* 8:e62760.
13. Nelson BR, et al. (2013) Skeletal muscle-specific T-tubule protein STAC3 mediates voltage-induced Ca2+ release and contractility. *Proc Natl Acad Sci USA* 110:11881–11886.
14. Horstick EJ, et al. (2013) Stac3 is a component of the excitation-contraction coupling machinery and mutated in native American myopathy. *Nat Commun* 4:1952.
15. Polster A, Perni S, Bichraoui H, Beam KG (2015) Stac adaptor proteins regulate trafficking and function of muscle and neuronal L-type Ca2+ channels. *Proc Natl Acad Sci USA* 112:602–606.
16. Polster A, Nelson BR, Olson EN, Beam KG (2016) Stac3 has a direct role in skeletal muscle-type excitation-contraction coupling that is disrupted by a myopathy-causing mutation. *Proc Natl Acad Sci USA* 113:10986–10991.
17. Linsley JW, et al. (2017) Congenital myopathy results from misregulation of a muscle Ca2+ channel by mutant Stac3. *Proc Natl Acad Sci USA* 114:E228–E236.
18. Campiglio M, Flucher BE (2017) STAC3 stably interacts through its C1 domain with CaV1.1 in skeletal muscle triads. *Sci Rep* 7:41003.
19. Kurochkina N, Guha U (2013) SH3 domains: Modules of protein-protein interactions. *Biophys Rev* 5:29–39.
20. Tanabe T, Beam KG, Adams BA, Niidome T, Numa S (1990) Regions of the skeletal muscle dihydropyridine receptor critical for excitation-contraction coupling. *Nature* 346:567–569.
21. Nakai J, Tanabe T, Konno T, Adams B, Beam KG (1998) Localization in the II-III loop of the dihydropyridine receptor of a sequence critical for excitation-contraction coupling. *J Biol Chem* 273:24983–24986.
22. Kugler G, Weiss RG, Flucher BE, Grabner M (2004) Structural requirements of the dihydropyridine receptor alpha1S II-III loop for skeletal-type excitation-contraction coupling. *J Biol Chem* 279:4721–4728.
23. Dinkel H, et al. (2016) ELM 2016–Data update and new functionality of the eukaryotic linear motif resource. *Nucleic Acids Res* 44:D294–D300.
24. Wilkens CM, Kasielke N, Flucher BE, Beam KG, Grabner M (2001) Excitation-contraction coupling is unaffected by drastic alteration of the sequence surrounding residues L720-L764 of the alpha 1S II-III loop. *Proc Natl Acad Sci USA* 98:5892–5897.
25. Lau K, Van Petegem F (2014) Crystal structures of wild type and disease mutant forms of the ryanodine receptor SPRY2 domain. *Nat Commun* 5:5397.
26. Stamm DS, et al. (2008) Native American myopathy: Congenital myopathy with cleft palate, skeletal anomalies, and susceptibility to malignant hyperthermia. *Am J Med Genet A* 146A:1832–1841.
27. Bannister RA (2016) Bridging the myoplasmic gap II: More recent advances in skeletal muscle excitation-contraction coupling. *J Exp Biol* 219:175–182.
28. Grabner M, Dirksen RT, Suda N, Beam KG (1999) The II-III loop of the skeletal muscle dihydropyridine receptor is responsible for the bi-directional coupling with the ryanodine receptor. *J Biol Chem* 274:21913–21919.
29. Bannister RA, Papadopoulos S, Haarmann CS, Beam KG (2009) Effects of inserting fluorescent proteins into the alpha1S II-III loop: Insights into excitation-contraction coupling. *J Gen Physiol* 134:35–51.
30. Van Petegem F, Clark KA, Chatelain FC, Minor DL, Jr (2004) Structure of a complex between a voltage-gated calcium channel beta-subunit and an alpha-subunit domain. *Nature* 429:671–675.
31. Grabner M, Dirksen RT, Beam KG (1998) Tagging with green fluorescent protein reveals a distinct subcellular distribution of L-type and non-L-type Ca2+ channels expressed in dysgenic myotubes. *Proc Natl Acad Sci USA* 95:1903–1908.
32. Kabsch W (2010) Xds. *Acta Crystallogr D Biol Crystallogr* 66:125–132.
33. Adams PD, et al. (2010) PHENIX: A comprehensive Python-based system for macromolecular structure solution. *Acta Crystallogr D Biol Crystallogr* 66:213–221.
34. McCoy AJ, et al. (2007) Phaser crystallographic software. *J Appl Cryst* 40:658–674.
35. Emsley P, Lohkamp B, Scott WG, Cowtan K (2010) Features and development of coot. *Acta Crystallogr D Biol Crystallogr* 66:486–501.
36. Murshudov GN, et al. (2011) REFMAC5 for the refinement of macromolecular crystal structures. *Acta Crystallogr D Biol Crystallogr* 67:355–367.
37. Powell JA, Petherbridge L, Flucher BE (1996) Formation of triads without the dihydropyridine receptor alpha subunits in cell lines from dysgenic skeletal muscle. *J Cell Biol* 134:375–387.
38. Barrett CF, Tsien RW (2008) The Timothy syndrome mutation differentially affects voltage- and calcium-dependent inactivation of $Ca_V1.2$ L-type calcium channels. *Proc Natl Acad Sci USA* 105:2157–2162.